

# Computational Investigation of the Pressure and Skin Friction Coefficient Distribution on a Mixed Hypersonic Inline Intake with Blunt Nose

Dr. V.B. Jaware

Professor

Department of Mechanical Engineering  
Rajarshi Shahu College of Engineering, University of Pune  
Pune – 411 044, Maharashtra, India.

Dr. J.A. Hole

Professor

Department of Mechanical Engineering  
Rajarshi Shahu College of Engineering, University of Pune  
Pune – 411 044, Maharashtra, India

Dr. Amarjit Singh

Associate Director

Terminal Ballistics Research Laboratory  
Chandigarh, India

**Abstract**--A study has been carried out to find out the flowfield inside a three dimensional hypersonic intake with different nose bluntness using commercial computational fluid dynamics software. This study has been carried out for a free stream Mach number of 6.5, a unit Reynolds number  $1.6 \times 10^6$  per meter with an intake contraction ratio of 2.88. The purpose of this analysis was to investigate the effect of nose bluntness on the external and internal compression in a mixed compression inline intake. An intake models with different nose bluntness has been analyzed using 3-D numerical simulations based on a commercially available CFD code. The CFD code and the turbulence model used is validated by comparing the experimental results available in literature with computational results. Computational results show that the nose bluntness has significant influence on pressure distribution on hypersonic intake. Nose bluntness affects the shock wave/boundary layer interactions on intake upper surface significantly. Numerical results of three dimensional simulations are also compared with two dimensional numerical simulations to study the effect of third dimensions on internal and external compression.

**Keywords:** *Inline Intake, Intake Fence, Scramjet, Nose Bluntness, Hypersonic Flow*

\*\*\*\*\*

## I. INTRODUCTION

Intake of a hypersonic vehicle has a major role on the overall performance of its air breathing propulsion system. The main function of an intake is to provide the homogeneous high pressure flow to the engine with minimum aerodynamic losses. External compression is performed through forebody and ramp shocks outside the intake and internal compression through a series of oblique shocks inside the intake. Based on the plane in which internal compression takes place, two types of intake designs are possible - one where the internal compression occurs in the same plane as the forebody compression, and the

other where internal compression takes place in a plane perpendicular to the forebody compression. The former type of intake is called inline compression intake and the later is termed as sidewall compression intake. The external compression of the flow before entering an intake essentially takes place in vertical plane through the forebody bow shock and one or more ramp shocks.

Most of the open literature available is about sidewall compression intake. Experimental and numerical studies [5-6-7] show the effect of intake geometric parameters on the performance and detailed flow structure through sidewall-compression intake. Besides various other requirements, intake should start at low Mach number, operate over a wide Mach

number range, and should work efficiently at designed Mach number [17]. However, fixed geometry intakes can only be used over a relatively narrow range of Mach numbers while variable geometry intakes can be used over wide range of Mach numbers with a reasonably good pressure recovery [21]. Compression process in an inline intake can be approximated to be two-dimensional in comparison to the three-dimensional in a sidewall compression intake. Three dimensional fixed geometry sidewall compression intakes have better performance than the two dimensional inline intakes over a relatively wide range of Mach numbers. However, it has relatively lower mass flow rate and pressure recovery at design Mach number and more complex flowfield [16]. Sanator et al [20] conducted experimental investigation to study the effects of leading edge bluntness on boundary layer separation using surface pressure measurements. Their tests investigated that the introduction of leading edge bluntness to 2D-inlet type flows at  $M_\infty = 10.55$  and  $Re_\infty/cm = 6.1 \times 10^4$  promoted separation. This promotion of separation was attributed to the reduced boundary layer edge Mach number. Townsend [22] conducted pressure measurements upstream of the hingeline on a blunted flat plate / flap configuration ( $d = 5.0$  mm) at  $M_\infty = 10.0$  and  $Re_\infty/cm = 5.0 \times 10^4$ , showed an appreciable reduction in the extent of the separated flow region when leading edge bluntness was introduced. The state of the boundary layer was diagnosed as being entirely laminar. Danial Arnel et al [3] carried out review on laminar and turbulent boundary layer interaction with shock waves. There are no basic differences between Laminar and turbulent interactions as far as the overall flow topology is considered. Of course, turbulent interactions vary from laminar interactions in terms of scales, intensity of pressure rise and thermal effects. A shock wave turbulent boundary layer interaction raises difficult problems which are still largely unsolved. Considering above pros and cons and lack of published work, a study has been carried out to investigate the flow through an inline intake with different nose bluntnesses. The nose bluntness has significant influence on pressure distribution on different parts of the intake. Nose bluntness affects the shock wave/boundary layer interactions on intake upper surface significantly. Numerical results also indicate that the nose bluntness has a significant influence on boundary layer formed on vehicle forebody lower surface and intake upper surface.

## II. COMPUTATIONAL SETUP AND PROCEDURE

A sketch of the vehicle forebody with engine intake model with main dimensions is shown in Fig. 1. All dimensions have been non-dimensionalised using distance from vehicle nose to intake entry,  $F$ , of the vehicle.

A commercially available solver using cell-centered finite volume technique to solve the three dimensional, compressible Reynolds-Averaged Navier-Stokes equations code has been used. The implicit solver with an upwind discretisation scheme for convective term and second order central differencing scheme for diffusion terms in flow and transport equation for  $K-\epsilon$  turbulence model has been used. The

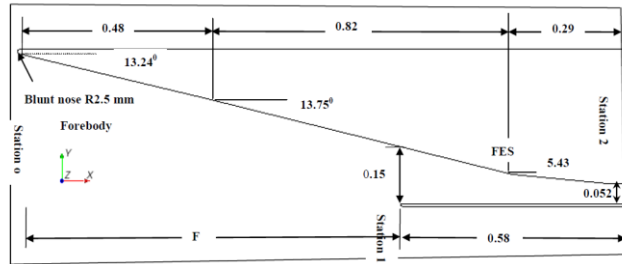


Fig. 1. A sketch of vehicle forebody and intake.

hypersonic free stream flow is defined by specifying the boundary conditions given in Table 1. The outflow being predominantly supersonic, the variables are completely extrapolated from interior to the outlet boundary. The air is assumed to be a calorically perfect gas with constant specific heat ratio,  $\gamma = 1.4$ . At solid walls no-slip adiabatic boundary condition is imposed.

Table 1. Inflow boundary conditions

Cases	$M_\infty$	$T_\infty$	$P_\infty$	$k_\infty$
Two dimensional intake with different nose radii	6.5	237K	830Pa	0.05

A rectangular computational domain was chosen for all the cases of different nose bluntness. The computations were performed on a 16 core cluster. The cluster was connected to a SAN to store large amount of data generated. To monitor convergence of the numerical solution, axial force, normal force and pitching moment plots were monitored. The solution converged after about 25,000 iterations. An additional criterion enforced in the current analysis required the difference between computed inflow and outflow mass to drop to 0.5%.

Analysis of grid sensitivity to study the influence of bluntness effect confirmed that the grid resolution used is sufficient to capture the relevant physical features. The axial force, normal force and pitching moment obtained with different grid refinement levels were compared. Coarse Mesh (total hexahedral cells 3, 85,851), medium mesh (total hexahedral cells 19, 94,337) and fine mesh (total hexahedral cells 34, 09,251), the maximum discrepancy between the three

mesh levels was found to be less than 3%. Figure 2 shows computed pressure along the vehicle forebody lower and the intake upper surface for these three grids. Out of these analyses, medium mesh was selected, and all results of nose bluntness cases are computed applying this resolution. To ensure the accuracy of turbulent flow solution, a value of  $Y^+$  below 20 is maintained in the main portion of the wall flow region required for this analysis.

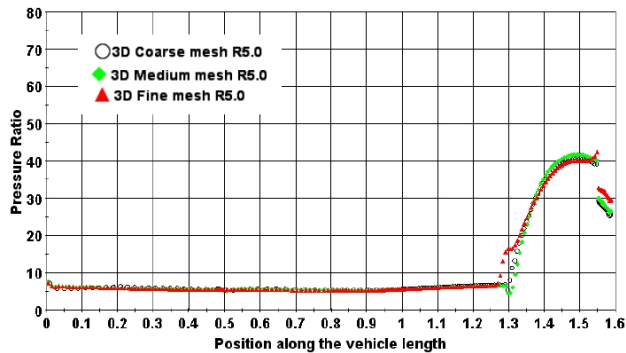


Fig. 2. Pressure distribution on forebody lower and the intake upper surface for different grids.

### III. Validation of Code

Suitability of the CFD solver to predict a complex high speed flow through a scramjet inlet was evaluated by comparing the results obtained by the present solver with the experimental results already available in the literature for flow through a dual-mode scramjet at Mach number 4 [19]. Figure 3 shows

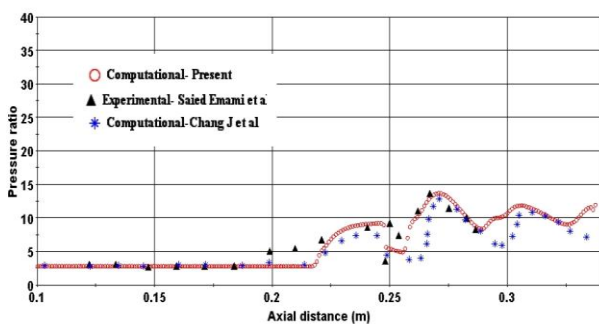


Fig. 3. Comparison of present computation with experimental and other computational results.

the comparison of variation of pressure along the ramp side of dual-mode scramjet at Mach number 4. The present computational results are also compared with computational result for the same geometry and flow conditions [12]. The present computational results show good agreement with the already available Saied experimental as well as computational results. However discrepancy on the ramp side pressure distribution can be observed in the shock boundary layer interaction region and expansion region. The probable reason for this discrepancy

could be deficiency of the turbulence model used, assumed calorically perfect gas condition and the differences between experimental and numerical simulation conditions or the

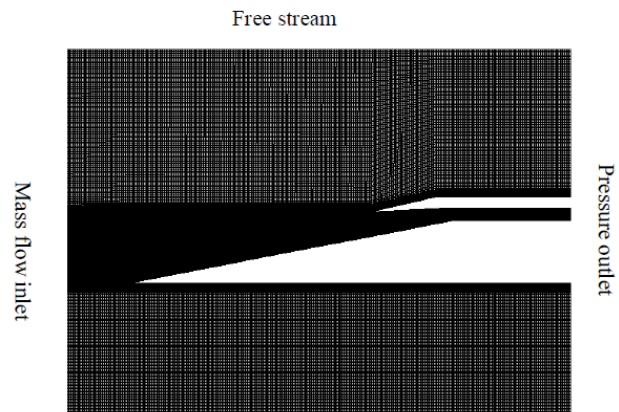


Fig. 4. Grid distribution.

measurement error of the sensors. It indicates the sufficiency of grid distribution, turbulence modeling, boundary conditions etc., being adopted in present computations. Based on reasonably good comparison achieved, further computations are made for present hypersonic intake geometry with similar grids, boundary conditions and turbulence modeling. Figure 4 shows a typical grid distribution showing the overall computational domain with necessary boundary conditions.

### IV. IV. RESULTS AND DISCUSSION

Three dimensional numerical simulations for six different nose radii have been carried out to obtain the static pressure distribution and skin friction distribution over different parts of the vehicle intake. To obtain further data about boundary layer condition and flowfield inside and outside the intake at different sections. Line probes are drawn in

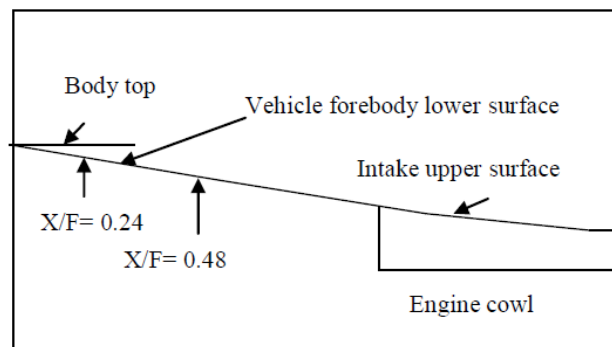


Fig. 4.1. Two dimensional sketch of mixed inline intake model with blunt nose.

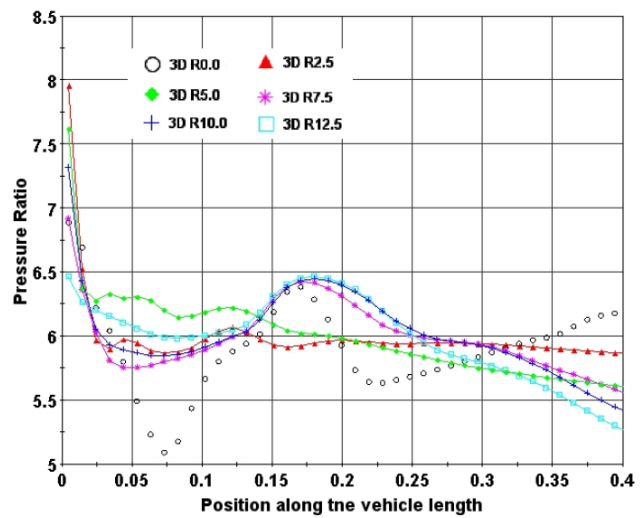
vertical direction as shown in Fig. 4.1. To study the effect of nose bluntness in the sonic line height of boundary layer two

vertical line probes are drawn from one near to leading edge of nose at  $X/F = 0.24$  and another at  $X/F = 0.48$  as shown in Fig. 4.1. In addition numerical Schlieren pictures, different contours were drawn to find out flow around the vehicle nose, internal and external shock structure of the intake. In a mixed compression intake, part of the compression takes place before the flow enters the intake through the forebody shock and the ramp shocks. The flow is processed through vehicle nose before it enters inside the intake. The growth of boundary layer at the sharp leading edge of vehicle generates weak leading edge oblique shock. This deflects the flow over vehicle body. By changing the nose from sharp to blunt, this oblique shock changes its shape from oblique to detached bow shock. The effect of nose bluntness by changing the nose radius is studied on external compression, internal compression and boundary layer formed on vehicle forebody lower and intake upper surface.

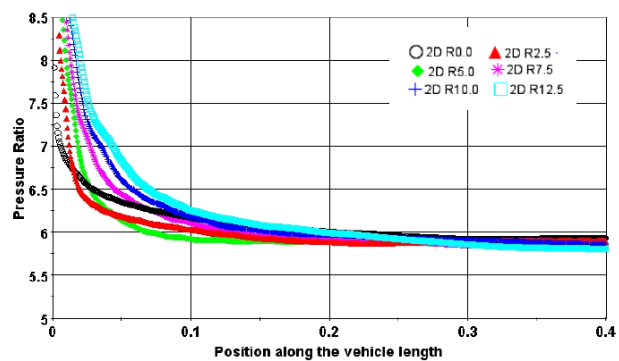
### Study of pressure distribution with different nose bluntness

The curved part of the bow shock in the vicinity of the blunt leading edge of the vehicle generates entropy layer, so that the streamlines passing through this curved part of the shock form the entropy layer. The pressure of air passing along these streamlines is first increased due to stronger portion of the shock wave and after this air expands towards the pressure of the sharp leading edge case in downstream direction. For air travelling along the streamlines, which are further displaced from the wall thus not passing through the curved portion of the shock, the pressure of air is only raised equivalent to oblique shock of sharp plate. Hence the streamlines passing

through the curved portion of the shock are responsible for the overpressure observed downstream of the vehicle leading edge as shown in Figure 4.2. In a similar fashion, pressure gradient of streamlines, passing through the curved portion of the shock represents the entropy layer. The decay of the overpressure approximately indicates that all streamlines of the entropy layer entered the boundary layer so that the entropy layer is swallowed [8]. To estimate the location of entropy layer swallowing or respectively the



(a) 3D Pressure distribution



(b) 2D pressure distribution

Fig. 4.3. Comparison of 3D and 2D pressure distributions downstream of the vehicle nose leading edge for different radii on vehicle's forebody lower surface.

level of the overpressure, the blast wave theory is to be employed. The blast wave theory predicating the overpressure extent indicates that entropy layer swallowing moves downstream with increased leading edge radius of the vehicle nose. Therefore, small leading edge bluntness causes the entropy layer being swallowed near the vehicle nose and for large bluntness the entropy layer is swallowed near to the intake entry. The Figure 4.3 shows comparison between the

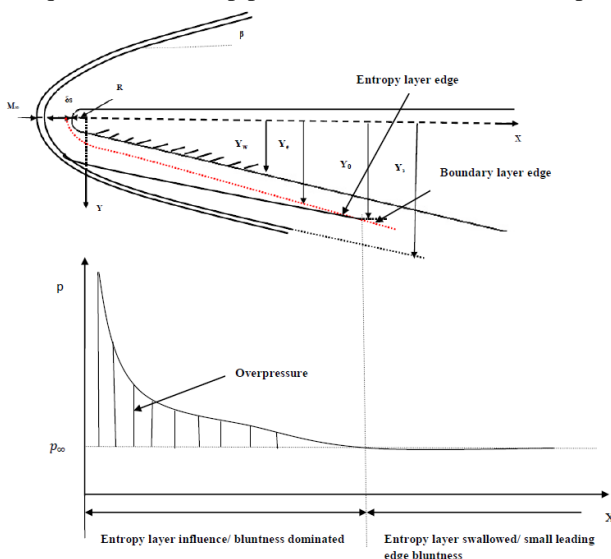


Fig. 4.2. Outline of entropy layer swallowing with corresponding pressure distribution[8].

flow fields with 2D and 3D pressure ratio variation over lower surface of the forebody along length of the vehicle at centerline for different nose radii. The flow over the lower side of the vehicle is processed through nose shock and ramp shock generated by the ramp.

2D simulation overestimates the pressure ratio as compared with 3D simulations. This indicates 3D effect shows a reduced pressure distribution over the vehicle forebody lower surface. 3D simulations show the non uniformities in the pressure distribution over the vehicle forebody lower surface. The pressure increase due to nose shock on lower surface is not showing increasing trends as observed in 2D simulations. Highest pressure raise on the vehicle forebody lower surface in 3D simulation is observed for 7.5 mm blunt leading edge nose. At the end of first ramp, drop in pressure is observed for all blunt leading edge cases, except the sharp nose case. Comparison of 2D and 3D numerical simulation indicates that the three dimensional flow field is more complex as compared to the two dimensional flow. It needs further detailed investigation to understand the flow field over the vehicle forebody lower surface in case of 3D flow.

**Study of sonic line height of the boundary layer for different nose bluntness**

The streamline close to the vehicle surface axis requires large deflections for blunt nose. As.

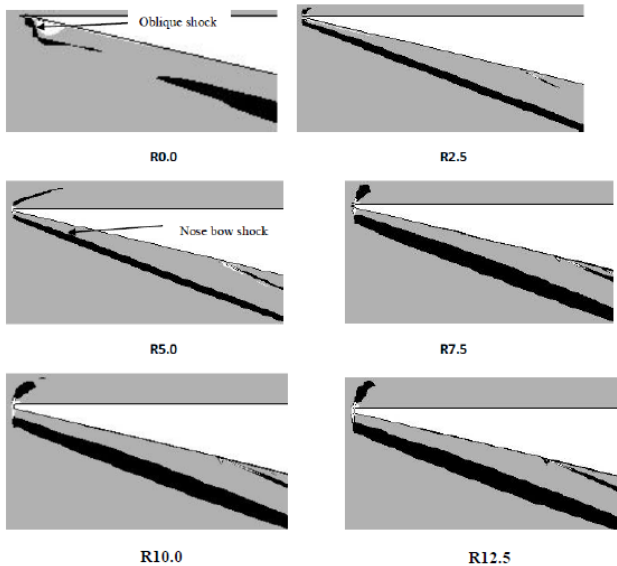


Fig. 4.5. 3D numerical Schlieren showing bow shock generated by different nose radii

bluntness increases streamline deflection from the body axis also increases. This is achieved by the formation of a strong near normal shock close to the surface which decelerates the flow to subsonic speeds, allowing it to negotiate the finite leading edge. Following this, the flow accelerates back to

supersonic speeds. Further turning downstream of the sonic line is achieved by Prandtl-Meyer expansion fans. Away from the body axis, deflection angle required is small. As a result, streamlines in this region of the flowfield are processed by weaker oblique shock waves. This phenomenon increases the detached bow shock angle generated by the

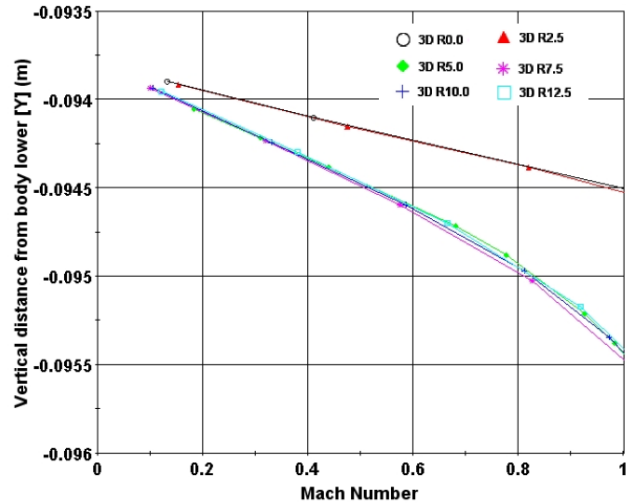


Fig. 4.6. 3D Mach number variation normal to free stream direction over forebody lower surface at stream wise location X/F=0.24

nose as the nose bluntness increases as shown in Fig.4.5. The entropy layer is generated by the curved part of the bow shock in the vicinity of the leading

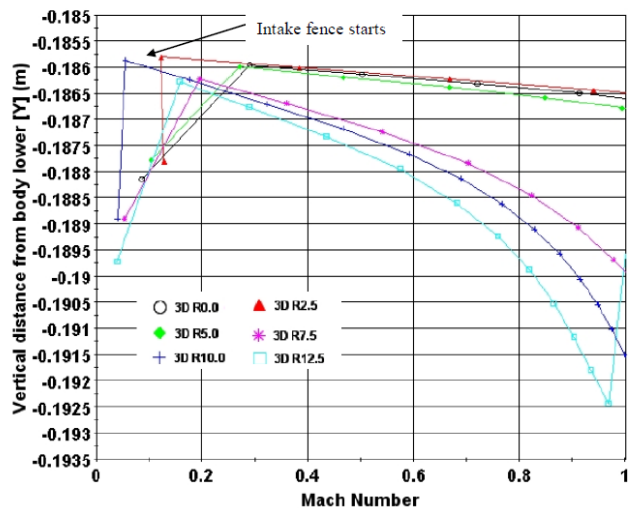


Fig. 4.7. 3D Mach number variation normal to free stream direction over forebody lower surface at stream wise location X/F = 0.48.

edge, so that the streamlines passing through this curved part of the shock form the entropy layer. The entropy layer thickness increases with the increase in nose bluntness. This increase in

entropy layer thickness changes the location of entropy layer swallowing points on vehicle's forebody lower surface. The streamlines passing through strong portion of the curved shock generate entropy layer and these streamline features higher static temperature before entropy layer swallowing point and after entropy layer swallowing point these streamlines are characterized by higher velocity and decreased temperatures. This variable strength streamline which passes through entropy layer generates variation in Mach number from normal to free stream flow direction over the vehicle's forebody lower surface at stream wise location at  $X/F = 0.24$  and  $X/F = 0.48$  as shown in Fig.4.6 and 4.7. The streamlines representing the entropy layer which passes through entropy layer and boundary layer before entropy layer swallowing increase the static temperature inside boundary layer and it decreases the velocity of air which is flowing through boundary layer. This increase in static temperature increases the sonic speed of the air which is flowing through boundary layer. This increase in sonic speed and decrease in local velocity of air which is travelling along with entropy layer streamline decreases the Mach number inside the boundary layer nearer to forebody lower surface. This decreased Mach number increases the sonic line height inside the boundary layer with increase in nose bluntness at stream wise position over the vehicle's forebody lower surface (Fig.4.6 and 4.7). It indicates that the sonic line height increases, the velocity gradient inside the sonic line portion near to the wall of the boundary layer decreases. This increase in sonic line height increases the boundary layer thickness and changes boundary layer edge conditions as compared with blunt leading edge case. Three dimensional numerical simulations show decrease in sonic line height as compared to two dimensional simulations [15]. Also non uniformities in Mach number distribution near to vehicle forebody lower surface at  $X/F = 0.48$  are observed in case of 3D computations from where the second ramp starts. In three dimensional intakes, from the same location sweptback intake fences start. The increase in sonic line height is less in case of 0.0, 2.5 and 5.0 mm nose leading edge radii cases as compared to other cases of nose bluntness at  $X/F = 0.24$ .

**Pressure distribution during cow bow shock / boundary layer interaction with different nose bluntness**

The cowl bow shock/ boundary layer interaction on intake upper surface is studied by using a simple flowfield model of SWBLI due to impinging shock wave on a boundary layer of a supersonic flat plate is shown schematically in Fig.4.8. This figure also displays the separation of boundary layer with corresponding separation and reattachment shock with separation bubble.

The upper boundary of the considered model is the streamline which would pass through the sonic point of the undistributed boundary layer at sonic height (sh). The sonic height is assumed to be the height of the sonic line of undistributed boundary layer upstream of the separation point. The entropy layer generated on the vehicle forebody lower surface influences the sonic line height of boundary layer for different nose bluntness. This effect is

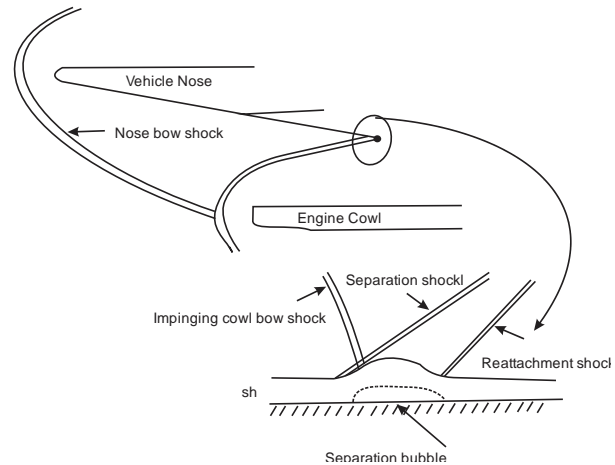


Fig. 4.8. Sketch of a shock wave/ boundary layer interaction with separation

discussed in earlier section in detail. How this sonic line height of boundary layer affect the shock wave/ boundary layer interaction in terms of separation length, separation pressure and reattachment pressure is discussed in details by observing the pressure variation on the intake upper surface and numerical Schlieren pictures as shown in Fig. 4.9 and 4.10. The flow over the intake upper

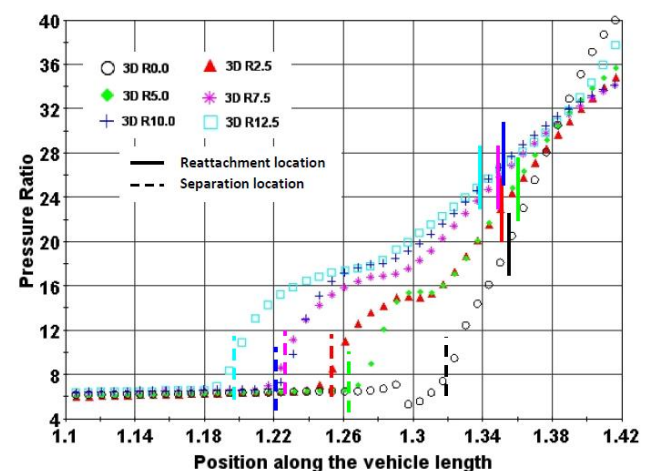


Fig. 4.9. 3D Pressure distributions for different radii on intake upper surface with separation and reattachment locations.

surface is processed through the impinging cowl shock, separation bubble expansion waves, separation shock, reattachment shock and two expansion fans due to expanding intake upper surface at  $X/F = 1.3$  and at  $X/F = 1.55$  just before the end of intake geometry. The shock wave/ boundary layer interaction over intake upper surface is influenced by nose bluntness effect as well as cowl shock strength. Again cowl shock strength depends on the flow conditions which are processed through nose shock, ramp shock and their entropy layer effect. The separation locations, reattachment locations, separation lengths and size of separation bubble during the shock wave/boundary layer interactions depend on boundary layer thickness before interaction, entropy layer swallowing point location and type of interaction between nose shock and cowl lip shock. The cowl shock impinges on the intake upper surface after nose and cowl shock interaction. Thus the strength of cowl shock is influenced by which Edney type of shock interference takes place, according to the location of nose shock impingement on cowl lip bow shock. Present investigation is concentrated on the effect of nose bluntness in terms of entropy layer, boundary layer thickness on shock wave/boundary layer interactions over the intake upper surface. The effect

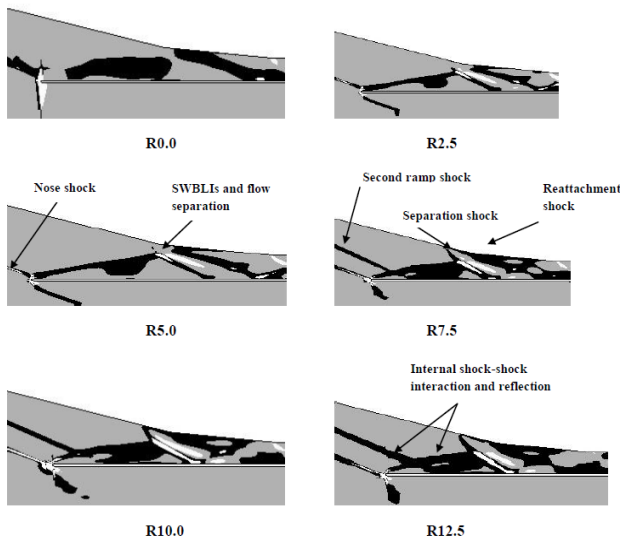


Fig. 4.10. 3D numerical Schlieren pictures for different nose radii over intake upper surface showing SWBLIs and internal shock reflection for different nose radii.

of increased nose radius is to increase and then decrease the separation length. The point of reversal depends on the cowl shock strength after nose shock and cowl shock interaction, free stream Mach number and nose radius. The vehicle nose and ramp shock interact with the cowl shock at different

portion of the cowl bow shock with different nose radii as shown in Fig. 4.10. The separation size increases from sharp nose case to blunt leading edge case with radius 2.5 mm case as shown in Table 2. The separation and reattachment locations for different nose bluntness cases are located from velocity contours and their corresponding locations are marked on pressure variation plot over the intake upper surface as show in Fig.4.9. This shows that for nose bluntness case of 5.0 mm radius, the separation length is decreased slightly and from nose bluntness radius 7.5 mm onwards the separation length is increased. Two dimensional computations show that the separation length reversal bluntness radius is 7.5 mm [15] and three dimensional computations show 5.00 mm radius case. The pressure distributions show the increased overpressure due to the increased leading edge radius upstream of the interaction so that for the large leading edge radii the induced pressure gradient reaches the boundary layer just upstream of the separation point. The increase in nose leading edge radius affects the pressure plateau region, separation pressure, and reattachment pressure and separation length. As nose bluntness increases its effect is to increase the separation

Table 2 3D details of sonic line height, separation locations, reattachment locations and separation length for different nose radii

R (mm)	sh (X/F=0.24) mm	sh (X/F=0.48) mm	S (mm)	R (mm)	S <sub>i</sub> (mm)
0.00	0.39	0.87	2210	2270	65
2.50	0.47	0.74	2093	2262	169
5.00	1.47	1.00	2128	2287	159
7.50	1.66	4.25	2055	2257	202
10.00	1.46	5.75	2030	2265	235
12.50	1.41	6.75	2069	2254	245

and reattachments pressures respectively. By observing internal shock reflection pattern from numerical Schlieren and pressure variation plot, it is observed that it is the highest reattachment pressure for sharp nose case. The reason for highest increase in pressure could be the strongest reattachment shock formed during shock wave/boundary layer interaction because the reattachment location is in downstream direction from the first expansion shoulder. In sharp nose case expansion waves come in contact with interacting cowl shock and these expansion waves may return as compression waves along with this shock and it's strength is to be increased. In other cases the reattachment shock comes in contact with expansion fans generated by the expansion shoulder at  $X/F = 1.3$ . This expansion fans reduces the pressure of reattachment shock for other cases. But for sharp nose case, shock reattachment location is after the expansion shoulder. The effect of increase in nose leading edge radius is to shift the separation and

reattachment in upstream direction as shown in Table 5.2. This indicates that the cowl bow shock wave angle increase with increase in leading edge radius and this increased shock angle shifts both locations in upstream direction. By comparing numerical Schlieren pictures of both the simulations, it is observed that in case three dimensional simulation nose shock and ramp shocks are not intersecting at one location. This phenomenon causes further complication in the internal compression.

### Pressure distribution on engine's cowl surface with different nose bluntness

The pressure ratio variation distribution on the engine cowl surface is shown in Fig. 4.11. As nose bluntness increases the initial pressure on the engine cowl surface increases slightly with increase in bluntness. Observation of pressure distribution indicates the impingement of separation and reattachment shock formed during the shock wave/boundary layer interactions impinges on the cowl at

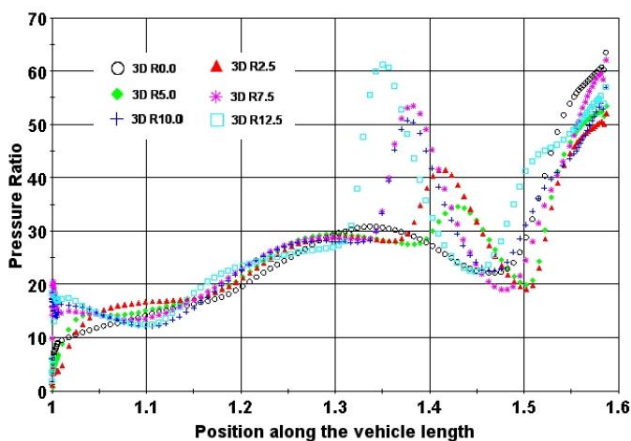


Fig. 4.11. 3D computed pressure distributions for different nose radii on engine cowl surface.

different locations. This produces increase in pressure at different locations on the engine cowl surface. In 12.5 mm nose bluntness case, the separation shock produces maximum increase in pressure on the engine cowl surface. Then this pressure rise reduces gradually from higher bluntness to lower.

## V. SUMMARY AND CONCLUSIONS

Computational investigations of turbulent, compressible, 3-D viscous flow in the hypersonic intake for various nose radii are presented. The numerical methodology has been validated by simulating the external and internal flow of dual mode scramjet intake and comparing with experimental data.

Three dimensional simulations under predicted the pressure over different component of the intake with increase in nose bluntness, in comparison to 2D simulation. In case of two dimensional simulations pressure distribution was observed to be uniform as compared with three dimensional simulations. This non uniform distribution may be because of three dimensional effects on pressure distributions. Decrease in separation lengths were observed in two dimensional simulations as compared with three dimensional simulations. Near to nose higher increase in sonic line height is observed in case of 2D simulations as compared with 3D simulations. From the starting of second ramp increase in sonic line height is seen in case of three dimensional simulations as compared to 2D simulations. It indicates the influence of fence shock on sonic line height.

## Nomenclature

- CFD = computational fluid dynamics
- D = dimensional
- F = distance from vehicle nose to intake entry
- M = Mach number
- FES = first expansion shoulder
- S = separation location
- R = reattachment location
- $S_1$  = separation length
- sh = sonic line height
- R = Nose radius
- H = intake height

## Subscript

- t = total condition
- 0 = free stream (Station 0)
- 1 = intake entry (station1)
- 2 = intake exit (station2)
- $\infty$  = free stream

## Acknowledgement:

Authors are grateful to BCUD, University of Pune, Pune for supporting this research work.

## References

- [1] Amarjit Singh et al., 1995. "Experimental investigation of hypersonic flow over a wing-body combination", AIAA-95-6083, Presented at AIAA sixth international aerospace planes and hypersonic technologies conference, Chattanooga, TN, USA.
- [2] Chang et al., 2008. "A CFD assessment of classifications for hypersonic inlet start/unstart phenomena" The aeronautical Journal, volume 113, No 1142.

- [3] Daniel et al., 2004: SWBLI, NATO.
- [4] Delery et al., 1999. "Shock phenomena in high speed aerodynamics: Still a source of major concern". The Aeronautical Journal, vol.103, Paper No.1019, pp 19-34.
- [5] Goonko et al., 2003. "Structure of flow over a hypersonic intake with sidewall wedges". AIAA Journal, Vol.41, No.3, pp 436-447.
- [6] Holland et al., 1993. "An experimental parametric study of geometric, Reynolds number and specific heats effects in three dimensional sidewall compression Scramjet intakes at Mach 6". AIAA Paper 93-0740.
- [7] Holland et al., 1995 "Computational parametric study of sidewall-compression scramjet inlet performance at Mach 10". NASA Technical Memorandum 4411.
- [8] Hirschel et al., 2005. "Basics of Aerothermodynamics" Springer Verlag, Berlin
- [9] Jaware et al., 2009. "Numerical simulation of internal flowfield in a 2D and a 3D hypersonic mixed inline intake at Mach 6.5.", International Conference on "Latest Trends in Simulation Modelling and Analysis (COSMA2009)", Proceedings of National Institute of Technology Calicut, Calicut, Kerala, India, VITF 76, pp 422-425.
- [10] Jaware et al., 2009. "A computational study of effect of intake fence on the performance of hypersonic vehicle inlet". Proceedings of Thirty Sixth National Conference On "Fluid Mechanics and Fluid Power (NCFMFP2009)", Government College of Engineering, Shivaji Nagar, Pune, India , pp237-243.
- [11] Jaware et al., 2009 "A computational study of internal flowfield investigation of a hypersonic vehicle inlet at mach 6.5." Proceedings of National Conference on "Modelling and Simulation (NCMS2009)", Defence Institute of Technology, Girinagar, Pune, India,
- [12] Jaware et al., 2010. "Numerical simulation of internal flowfield and performance evaluation of a 3D mixed inline intake with fence", Proceedings of International Conference on Advances in Mechanical Engineering (ICAME-2010)" held at S. V. National Institute of Technology (SV NIT), India, pp 332-326.
- [13] Jaware et al., 2011. "Computational study of the effect of fence on the external and internal compression in a mixed inline intake" International Review of aerospace Engineering (IRSE) Vol. 4, No.2, pp 35-42.
- [14] Jaware et al., 2011. "Numerical simulation of external and internal flowfield of a 3D mixed inline intake with strake" Proceeding of national conference on 'Advances in Engineering, Management and General sciences', Pimpri-Chinchwad College of Engineering, Pune, India.
- [15] Jaware et al., S.V. 2012 "Computational investigation of the effect of nose bluntness on the external and internal compression in a mixed inline intake" International Journal of Mechanical Engineering & Technology (IJMET), Vol. 3, No.01, pp 161-178.
- [16] Liang et al., 2008. "Performance enhancement of three-dimensional hypersonic inlet with sidewall compression". Proc. I Mech Vol.222 Part G: J. Aerospace Engineering, pp1121- 1219.
- [17] Mahapatra et al., 2008. "Shock tunnel studies on cowl/ramp interactions in generic scramjet intake". Journal of Aerospace Engineering, Vol.222, pp 1183-1191.
- [18] Mahapatra et al., 2009. "Studies on unsteady shock interactions near a generic scramjet intake." AIAA Journal, Vol. 47, No.9, pp 2223-2231.
- [19] Saied et al 1995 "Experimental investigation of inlet-isolator combustor for a dual mode scramjet at a Mach number of 4." NASA Technical paper 3501
- [20] Sanator et al., 1968. "Effects of Bluntness on Hypersonic Two-Dimensional Inlet type Flows." NASA CR-1145.
- [21] Sivkumar et al., 2006. "Numerical simulation of flow in a 3-D supersonic at higher Mach number". Defence Science Journal, Vol.56, No.4, pp 465-476.
- [22] Townsend 1990. "The Effects of Leading Edge Bluntness and Ramp Deflection Angle on Laminar Boundary Layer Separation in Hypersonic Flow" NASA TN-D 3290.